

# Thermal and Kerr nonlinear properties of plasma-deposited silicon nitride/ silicon dioxide waveguides

Kazuhiro Ikeda\*, Robert E. Saperstein, Nikola Alic and Yeshaiahu Fainman

*Department of Electrical and Computer Engineering, University of California, San Diego,  
9500 Gilman Drive, La Jolla, California 92093-0409*

*\*Corresponding author: [kaziked@ucsd.edu](mailto:kaziked@ucsd.edu)*

<http://emerald.ucsd.edu>

**Abstract:** We introduce and present experimental evaluations of loss and nonlinear optical response in a waveguide and an optical resonator, both implemented with a silicon nitride/ silicon dioxide material platform prepared by plasma-enhanced chemical vapor deposition with dual frequency reactors that significantly reduce the stress and the consequent loss of the devices. We measure a relatively small loss of  $\sim 4$  dB/cm in the waveguides. The fabricated ring resonators in add-drop and all-pass arrangements demonstrate quality factors of  $Q=12,900$  and  $35,600$ . The resonators are used to measure both the thermal and ultrafast Kerr nonlinearities. The measured thermal nonlinearity is larger than expected, which is attributed to slower heat dissipation in the plasma-deposited silicon dioxide film. The  $n_2$  for silicon nitride that is unknown in the literature is measured, for the first time, as  $2.4 \times 10^{-15} \text{ cm}^2/\text{W}$ , which is 10 times larger than that for silicon dioxide.

©2008 Optical Society of America

**OCIS codes:** (130.3130) Integrated optics materials; (160.4330) Nonlinear optical materials; (130.3990) Micro-optical devices

---

## References and links

1. V. R. Almeida, C. A. Barrios, R. R. Panepucci and M. Lipson, "All-optical control of light on a silicon chip," *Nature* **431**, 1081-1084 (2004).
2. T. Tanabe, M. Notomi, S. Mitsugi, A. Shinya and E. Kuramochi, "All-optical switches on a silicon chip realized using photonic crystal nanocavities," *Appl. Phys. Lett.* **87**, 151112 (2005).
3. K. Ikeda and Y. Fainman, "Nonlinear Fabry-Perot resonator with a silicon photonic crystal waveguide," *Opt. Lett.* **31**, 3486-3488 (2006).
4. K. Ikeda and Y. Fainman, "Material and structural criteria for ultra-fast Kerr nonlinear switching in optical resonant cavities," *Solid-State Electron.* **51**, 1376-1380 (2007).
5. T. Tanabe, K. Nishiguchi, A. Shinya, E. Kuramochi, K. Yamada, T. Tsuchizawa, T. Watanabe and H. Fukuda, "Fast all-optical switching using ion-implanted silicon photonic crystal nanocavities," *Appl. Phys. Lett.* **90**, 031115 (2007).
6. K. Ikeda, Y. Shen and Y. Fainman, "Enhanced optical nonlinearity in amorphous silicon and its application to waveguide devices," *Opt. Express* **15**, 17761-17771 (2007).
7. Q. Lin, O. J. Painter and G. P. Agrawal, "Nonlinear optical phenomena in silicon waveguides: modeling and applications," *Opt. Express* **15**, 16604-16644 (2007).
8. W. Stutius and W. Streifer, "Silicon nitride films on silicon for optical waveguides," *Appl. Opt.* **16**, 3218-3222 (1977).
9. C. H. Henry, R. F. Kazarinov, H. J. Lee, K. J. Orlowsky, and L. E. Katz, "Low loss  $\text{Si}_3\text{N}_4$ - $\text{SiO}_2$  optical waveguides on Si," *Appl. Opt.* **26**, 2621-2624, (1987).
10. N. Daldosso, M. Melchiorri, F. Riboli, M. Girardini, G. Pucker, M. Crivellari, P. Bellutti, A. Lui and L. Pavesi, "Comparison Among Various  $\text{Si}_3\text{N}_4$  Waveguide Geometries Grown Within a CMOS Fabrication Pilot Line," *J. Lightwave Technol.* **22**, 1734-1740 (2004).

11. T. Barwicz, M. A. Popovic, M. R. Watts, P. T. Rakich, E. P. Ippen and H. I. Smith, "Fabrication of Add-Drop Filters Based on Frequency-Matched Microring Resonators," *J. Lightwave Technol.* **24**, 2207-2218 (2006).
12. E. P. van de Ven, I-W. Connick, and A. S. HARRUS, "Advantages of dual frequency PECVD for deposition of ILD and passivation films," *Proc. IEEE VLSI Multilevel Interconnection Conference (VMIC)*, 194-201 (1990)
13. M. Notomi, A. Shinya, S. Mitsugi, G. Kira, E. Kuramochi and T. Tanabe, "Optical bistable switching action of Si high-Q photonic-crystal nanocavities," *Opt. Express*, **13**, 2678-2687 (2005).
14. M. Sheik-Bahae, A. A. Said, T.-H. Wei, D. J. Hagan and E. W. Van Stryland, "Sensitive measurement of optical nonlinearities using a single beam," *IEEE J. Quantum Electron.* **26**, 760-769 (1990).
15. C. A. Carter and J. M. Harris, "Comparison of models describing the thermal lens effect," *Appl. Opt.* **23**, 476-481 (1984).
16. W. Henschel, Y. M. Georgiev and H. Kurz, "Study of a high contrast process for hydrogen silsesquioxane as a negative tone electron beam resist," *J. Vac. Sci. Technol. B* **21**, 2018-2025 (2003).
17. L. F. Stokes, M. Chodorow and H. J. Shaw, "All-single-mode fiber resonator," *Opt. Lett.* **7**, 288- 290 (1982)
18. A. Boskovic, S. V. Chernikov, J. R. Taylor, L. Gruner-Nielsen and O. A. Levring, "Direct continuous-wave measurement of  $n_2$  in various types of telecommunication fiber at 1.55  $\mu\text{m}$ ," *Opt. Lett.* **21**, 1966-1968 (1996).

## 1. Introduction

Numerous nonlinear all-optical switching devices have been recently demonstrated with resonant cavities on silicon chips [1, 2], where the efficiency of weak nonlinearity of silicon is greatly enhanced due to the accumulated intensity and phase inside the resonant cavities. It has been shown experimentally [1, 2], numerically [2] and analytically [3, 4] that the switching operations in silicon occur due to dominant free carrier nonlinearity excited via two-photon absorption (TPA) as opposed to weaker but ultra-fast Kerr nonlinearity. Therefore, the demonstrated silicon-based nonlinear resonant devices have response time limited by the free carrier lifetime ( $>100\text{ps}$ ). In order to achieve faster operation in such resonator-enhanced nonlinear devices, we need to identify a new waveguide material with a shorter carrier lifetime [5, 6] or with a negligible TPA coefficient (i.e., wide energy bandgap), which should be also compatible with the standard silicon fabrication process. In this paper, we investigate silicon nitride (SiN) as a candidate material to achieve this objective, because its relatively larger refractive index than silicon dioxide ( $\text{SiO}_2$ ) results in small waveguide dimensions and its large energy bandgap gives a negligible TPA coefficient. This material will be also useful in pure Kerr nonlinear processes in a long interaction scheme without resonant structures since in silicon these devices are often limited by the nonlinear loss incurred by the generation of carriers and TPA [7]. Moreover, extensive researches in silicon photonics have been so far focused on using silicon-on-insulator substrates where the buried oxide layer is used as the under cladding and the crystalline silicon layer as the waveguide cores. This assumes that the photonic circuits are integrated in a single layer shared with electronic circuits. However, for more flexible and efficient integration, three dimensional multi-layer structures will be necessary, and SiN is one of the potential candidates because it is prepared by deposition processes. This material can be deposited by either low pressure chemical vapor deposition (LPCVD) at  $\sim 800^\circ\text{C}$ , or plasma-enhanced chemical vapor deposition (PECVD) at  $\sim 400^\circ\text{C}$ . Although these are both accessible equipments in the standard silicon fabrication process, PECVD will be more attractive for various applications due to the low process temperature. Several works on optical waveguide applications using SiN films prepared by LPCVD [8-11] have been reported. However, to the best of our knowledge, no work with the films by PECVD has been reported due to the basic drawback of large tensile stress resulting in undesirable cracks [8]. Here, we present a SiN/ $\text{SiO}_2$  waveguide and a resonator using materials prepared by PECVD with dual frequency reactors that can

significantly reduce the stress [12], and we also evaluate the nonlinear response of this material.

## 2. Fabrication of SiN/SiO<sub>2</sub> waveguide and resonator

We begin with depositing a 3 $\mu\text{m}$ -thick SiO<sub>2</sub> under-cladding layer on a silicon substrate, followed by deposition of a 500nm-thick SiN core layer, using an Oxford Plasmalab PECVD system where stress of the SiN film is controlled by alternating between RF and low frequency plasmas during the deposition. The SiO<sub>2</sub> film is deposited with the gas mixture of 5% SiH<sub>4</sub> diluted by N<sub>2</sub> (170sccm) and NO<sub>2</sub> (710sccm), the process pressure of 1000mT, the process temperature of 350°C, and the plasma frequency of 13.56MHz (20W, RF only). The SiN film is deposited with the gas mixture of 5% SiH<sub>4</sub> diluted by N<sub>2</sub> (400sccm), NH<sub>3</sub> (22sccm) and N<sub>2</sub> (600sccm), the process pressure of 650mT, the process temperature of 350°C, and the plasma frequencies alternating between 13.56MHz (20W, 13s) and 100kHz (20W, 7s). The refractive indexes of the fabricated films of SiN and SiO<sub>2</sub> are around 1.99 and 1.46, respectively. We next perform e-beam lithography with 30kV acceleration voltage using PMMA lift-off process to make a Ni hard mask pattern on top of the SiN film. Then, a reactive ion etching (RIE) with the gas mixture of CHF<sub>3</sub> (16sccm) and O<sub>2</sub> (3sccm) [11], the process pressure of 30mT, and the RIE power of 100W is used to define the SiN waveguide with 1 $\mu\text{m}$  width. After the Ni mask is removed, a 2 $\mu\text{m}$ -thick SiO<sub>2</sub> upper-cladding layer is deposited by the same process. Figures 1(a) and (b) show the SEM micrographs for the etched SiN waveguide before the upper-cladding deposition and the cross section of the waveguide after the deposition, respectively. We made an array of the waveguides with different lengths up to 5mm and measured the transmission loss of 4dB/cm for TE-like modes (see Fig. 1(c)), which is found comparable to those measured in waveguides prepared by LPCVD [8-11].

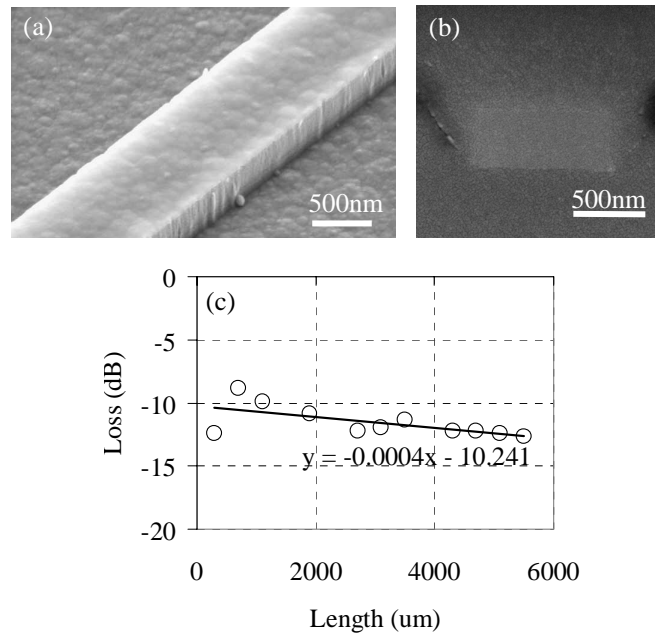


Fig. 1 SiN/SiO<sub>2</sub> waveguide: (a) and (b) SEM micrographs of the SiN/SiO<sub>2</sub> waveguides before and after the SiO<sub>2</sub> upper-cladding deposition, respectively. (c) Measured data and curve fit of propagation loss vs. waveguide length.

Using the same procedures, we fabricated add-drop type ring resonators with different bending radiuses ( $r=10, 15, 20\mu\text{m}$ ) and different gaps between the bus waveguides and the

rings ( $g=300, 500, 700\text{nm}$ ). We measured the transmission spectra of the fabricated devices using a broadband light source and a spectrum analyzer. Due to the relatively smaller index contrast than that in Si/SiO<sub>2</sub> waveguides, a tight bending in the SiN/SiO<sub>2</sub> waveguides results in a large bending loss. Consequently, we measured  $Q$  factors of 460, 8500 and 12900 for the ring resonators with  $r=10, 15$  and  $20\mu\text{m}$ , all with  $g=700\text{nm}$ . Smaller gaps resulted in smaller  $Q$  factors due to higher unloading losses into bus waveguides. Figures 2(a), (b) and (c) show the SEM micrograph of a ring resonator with  $r=20\mu\text{m}$  and  $g=700\text{nm}$ , the measured transmission spectrum, and the magnified spectrum for a resonance at  $1548\text{nm}$ , respectively.

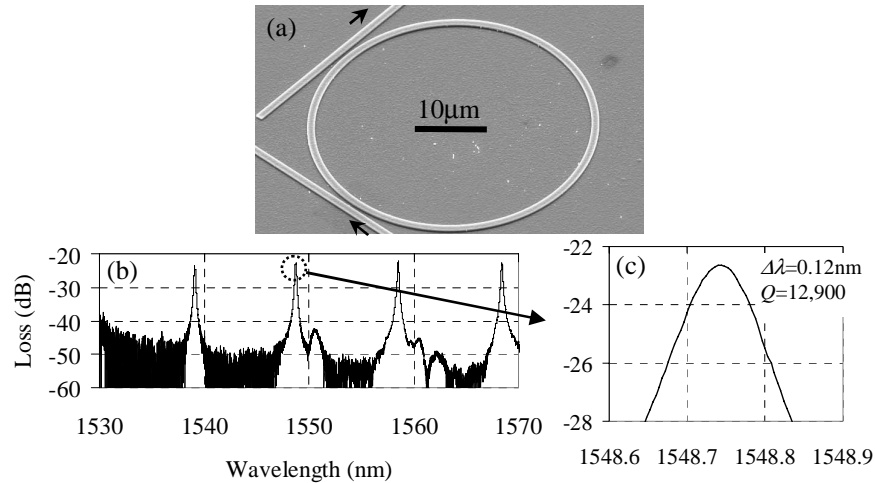


Fig. 2 Ring resonator with the SiN/SiO<sub>2</sub> waveguide ( $r=20\mu\text{m}$ ,  $g=700\text{nm}$ ): (a) SEM micrograph of the ring. (b) and (c) Transmission spectra.

### 3. Thermal nonlinearity

Next, we investigate the nonlinear response of our fabricated SiN/SiO<sub>2</sub> ring resonator with  $r=20\mu\text{m}$  and  $g=700\text{nm}$ . The first measurement uses a tunable continuous wave (CW) light source and a high power amplifier. Figure 3(a) shows the shift of the resonant peak wavelength as a function of the input power. We observe that the wavelength of the resonant transmission peak shifts to longer wavelength as the input power increases. Figure 3(b) shows the measured output power when the input power is kept constant at 23dBm and the wavelength is swept from shorter to longer wavelengths. This asymmetric response occurs due to the feedback from the ring resonator resulting in the bistable response as discussed in Ref. [13]. These nonlinear responses can be considered as either ultra-fast Kerr nonlinearity or accumulated thermal nonlinearity since both effects change the refractive index to a larger value (red shift). In order to determine which effect is responsible, we conduct a pump-probe experiment. We use a CW probe light of  $\sim 0\text{dBm}$  at  $1558\text{nm}$  to monitor the resonant transmission of the device in time, while the resonant device is optically modulated by a pump light of 23dBm at  $1548\text{nm}$  with slow and fast modulation frequencies of 100 kHz and 4 GHz. We obtained a clear probe modulation (see Fig. 3(c)) for the pump light modulated at 100kHz. However, we did not observe any probe modulation when we used a pump modulated at 4GHz. Therefore, we conclude that the nonlinearity we observed in these experiments corresponds to accumulated thermal nonlinearity.

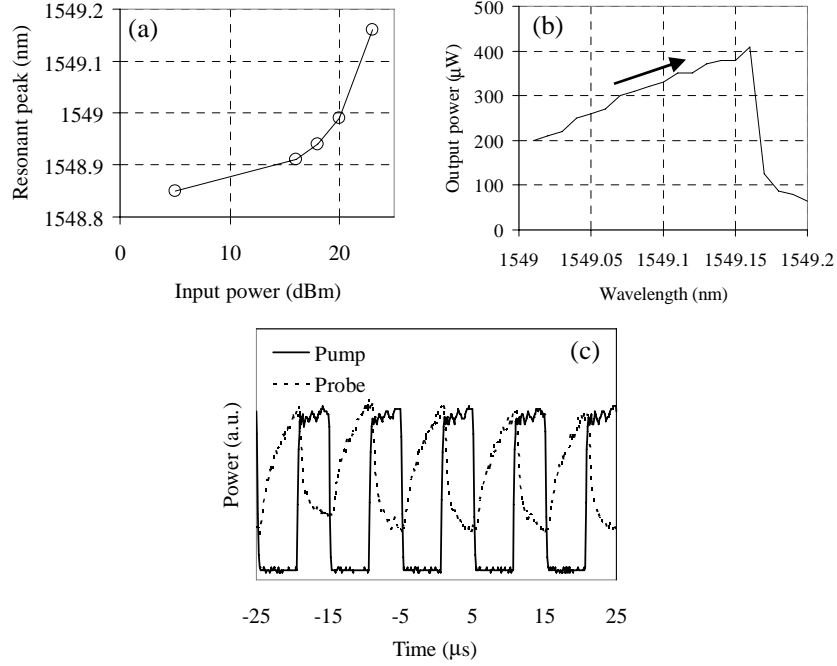


Fig. 3 Nonlinear response of the SiN/SiO<sub>2</sub> ring resonator: (a) and (b) Nonlinear responses with CW light, (c) Probe signal modulation by pump modulated at 100kHz.

We analyzed the thermal response of our fabricated device as follows. First, we estimate the group index  $n_g$ , the absorption coefficient  $\alpha$  inside the ring, and the coupling coefficient  $\kappa$  between the bus waveguide and the ring, by fitting the measured spectrum to an analytic formula of Fabry-Perot resonator. The estimated parameters are  $n_g=1.91$ ,  $\alpha=1.2\text{dB/mm}$  and  $\kappa=0.006$ . From these values, we can calculate the intensity enhancement inside the ring resonator at the resonant wavelength,

$$M = \frac{\kappa \cdot \exp\left(\frac{-\alpha L}{2}\right)}{2\left(1 - \sqrt{1 - \kappa \exp\left(\frac{-\alpha L}{2}\right)}\right)^2} = 7.2. \quad (1)$$

Thus, the peak power inside the ring resonator at the resonant wavelength can be estimated as 7.2 times the input power of 26dBm reduced by the coupling loss of 5dB (see Fig. 1(c)), corresponding to about 0.9W. And the measured probe modulation in Fig. 3(c) of 5.4dB corresponds to a refractive index change  $\Delta n$  of  $1.5 \times 10^{-4}$ . We then calculate the thermal accumulation using the rate equation with linear accumulation term  $\Delta n_a$  and heat dissipation decay term  $\Delta n/t_c$ ,

$$\frac{d\Delta n}{dt} = \Delta n_a - \frac{\Delta n}{t_c}. \quad (2)$$

The  $\Delta n_a$  and the characteristic time constant  $t_c$  are given by [14, 15]

$$\Delta n_a = \frac{(dn/dT) \cdot I \cdot \alpha}{2 \cdot \rho \cdot C_p}, \quad (3)$$

$$t_c = \frac{R_m^2 \cdot \rho \cdot C_p}{4 \cdot k} \quad (4)$$

where  $dn/dT$ ,  $I$ ,  $\rho$ ,  $C_p$ ,  $R_m$  and  $k$  are the thermo-optic effect, intensity, density, specific heat, mode radius and thermal conductivity, respectively. We use 4dB/cm for the  $\alpha$  in the Eq. (3) since the estimated value of 1.2dB/mm above will include the bending loss. We use the thermal parameters for fused silica in the literature because the SiN waveguide is surrounded by SiO<sub>2</sub> and  $dn/dT$  of SiN is unknown (i.e.  $dn/dT \sim 1 \times 10^{-5}$ ,  $\rho \sim 2.2 \text{g/cm}^3$ ,  $C_p \sim 0.76 \text{J/gK}$ , and  $k \sim 0.014 \text{W/cmK}$ ). The resultant plot for the time response of  $\Delta n$  is depicted by the red line in Fig. 4.

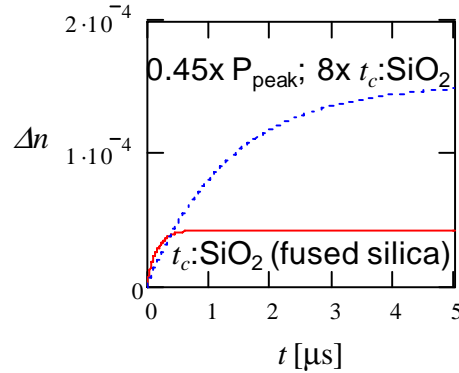


Fig. 4 Time response of  $\Delta n$  calculated with Eq. (2)

The calculated accumulation time is less than 1 $\mu$ s, which is much shorter than the measured response of > 5 $\mu$ s (see Fig. 3(c)). Also, the calculated steady state  $\Delta n$  is smaller than the measured value of  $1.5 \times 10^{-4}$ . If we use 8 times longer  $t_c$  and a smaller peak power (0.45 of the peak power right on resonance), the accumulation time and the index shift becomes close to the measured results as depicted by the blue line in Fig. 4. In fact, the peak intensity should be smaller than the value at the resonant wavelength because the resonant wavelength is slightly shifted by the induced index change. Therefore, the PECVD SiO<sub>2</sub> film probably has slower heat dissipation due to the high hydrogen content. Note that the uncertainty of the  $dn/dT$  of SiN only affects the steady state  $\Delta n$  but not the time constant  $t_c$ .

#### 4. Kerr nonlinearity

In order to observe the Kerr nonlinear response, we improved the SiN resonators by use of a negative resist [16] as the dry etching mask to achieve smoother sidewalls and decrease scattering loss, by removing the drop port to reduce the unloading loss, and by use of inverse tapers to reduce the coupling loss of the pump power. Figure 5(a) shows the transmission spectrum of the all-pass type ring resonator with  $r=20\mu\text{m}$  and  $g=600\text{nm}$ . As expected, we obtained a higher quality factor of about 35,600. We introduced a modulated pump and a CW probe in the same arrangement as in the previous pump-probe experiment, and detected 1GHz modulations as shown in Fig 5(b). Probe 1 and Probe 2 indicate the cases with the probe wavelength slightly shorter and slightly longer than that of the resonant transmission peak, respectively. Therefore, the modulation phases for these probes should be opposite to each other, as indeed can be observed from the experimental data in Fig. 5(b). Thus, we conclude that these modulations originate from the resonance shift by Kerr nonlinear effect. Now we estimate the  $n_2$  of the SiN film, which to the best of our knowledge is currently unknown in the literature. First we estimate the group index  $n_g$ , the absorption coefficient  $\alpha$  inside the ring, and the coupling coefficient  $\kappa$  between the bus waveguide and the ring by fitting the measured

spectrum to an analytic formula of all-pass type ring resonator [17]. The obtained parameters are  $n_g=1.91$ ,  $\alpha=1.6\text{dB/mm}$  and  $\kappa=0.009$ . The reason why the loss inside the ring was not improved is probably that the bending loss is dominant. Next, using these parameters and the equation for the intensity magnification factor  $M$  for the all-pass type ring resonator,

$$M = \frac{(1 - \kappa) \cdot \exp(-\alpha L)}{\left(1 - \sqrt{\kappa} \exp\left(\frac{-\alpha L}{2}\right)\right)^2}, \quad (5)$$

we estimated  $M=11.4$ . With the input peak power of 26dBm and the improved coupling loss of 2.5dB from fiber tip to the SiN waveguide and the estimated magnification factor of 11.4, we obtain the peak power of 2.6W inside the ring resonator. The measured modulation depth of 1.4% in Fig. 5(b) corresponds to 0.001nm of resonant wavelength shift, with which we calculate the corresponding index shift of  $1.2 \times 10^{-6}$ . Therefore,  $n_2$  of our SiN film is estimated as  $n_2 = \Delta n / I = 2.4 \times 10^{-15} \text{cm}^2/\text{W}$ , which is 10 times larger than that for SiO<sub>2</sub> [18]. This value would make sense because the  $n_2$  of SiN should be in between those of silicon and SiO<sub>2</sub> according to the refractive index and  $n_2$  scaling [4].

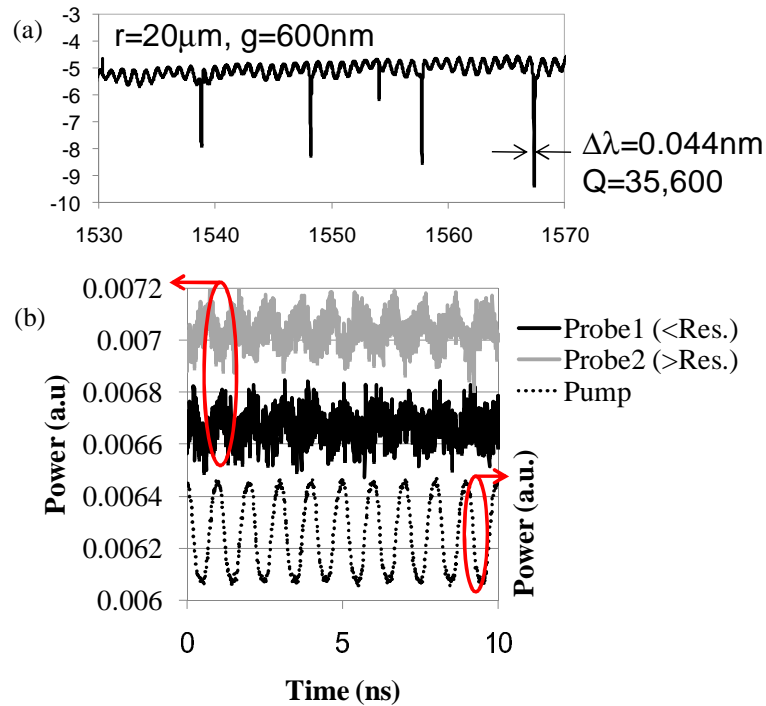


Fig. 5 All-pass type ring resonator with the SiN/SiO<sub>2</sub> waveguide ( $r=20\mu\text{m}$ ,  $g=600\text{nm}$ ): (a) transmission spectrum (b) Probe signal modulations by pump modulated at 1GHz.

## 5. Conclusions

We introduced and presented experimental evaluations of loss and nonlinear optical response in a waveguide and an optical resonator, both implemented with SiN/SiO<sub>2</sub> material platform prepared by PECVD with dual frequency reactors that significantly reduce the stress and the consequent loss in the fabricated devices. We measured a relatively small loss of  $\sim 4\text{dB/cm}$  in the SiN/SiO<sub>2</sub> waveguides. The fabricated ring resonators demonstrated experimentally measured quality factors of  $Q=12,900$  and  $35,600$ . The resonators were used to measure both the thermal and ultrafast Kerr nonlinearities. The measured thermal nonlinearity was larger

than expected, which was attributed to slower heat dissipation in the PECVD SiO<sub>2</sub>. The  $n_2$  for SiN that is unknown in the literature was measured for the first time as  $2.4 \times 10^{-15} \text{ cm}^2/\text{W}$ , which is 10 times larger than that for SiO<sub>2</sub>.

### **Acknowledgements**

Partial supports from the National Science Foundation, the Air Force Office of Scientific Research, and the Defense Advanced Research Projects Agency are gratefully acknowledged. K. Ikeda acknowledges the scholarship from the Nakajima Foundation, Japan.